CHINESE OPTICS LETTERS

Vol. 23, No. 1 | January 2025

Mode-selective edge coupler with cladding grating for a lithium-niobate-on-insulator waveguide

Pengfei Fan (范鹏飞), Xiaotian Zhang (张啸天), Chi Zhang (张 弛), Shanshan Cheng (成珊珊), Xiao-Hui Tian (田晓慧)*, Kunpeng Jia (贾琨鹏), Hua-Ying Liu (刘华颖)**, Shining Zhu (祝世宁), and Zhenda Xie (谢臻达)***

National Laboratory of Solid State Microstructures, College of Engineering and Applied Sciences, School of Electronic Science and Engineering, School of Physics, and Collaborative Innovation Center of Advanced Microstructures, Nanjing University, Nanjing 210093, China

*Corresponding author: tianxiaohui@nju.edu.cn

**Corresponding author: liuhuaying@nju.edu.cn

***Corresponding author: xiezhenda@nju.edu.cn

Received April 21, 2024 | Accepted July 24, 2024 | Posted Online February 4, 2025

Lithium-niobate-on-insulator (LNOI) chips have shown outstanding performance in various photonic devices including modulators, lasers, nonlinear converters, and quantum sources. LNOI-based edge couplers are quite important for further promotion of the above devices in practical applications, especially for large-scale multiport photonic uses, where efficient and mode-selective coupling between chips and fibers is of necessity. Previously, several LNOI edge couplers have been demonstrated, but they mainly focus on achieving high coupling efficiency of the fundamental mode, and sub-wavelength etched lithium-niobate (LN) structures are normally needed, which increases fabrication complexity. Here we propose a new type of edge coupler with direct mode-selective excitation ability, using only SiON cladding grating structures without additional etching of LN. By introducing a cladding waveguide with periodic structures on the uniform LNOI waveguide, high-efficiency excitation of multiple modes can be realized directly with easier fabrication. For a specific simulation here, TE_{00}, TM_{00}, and TE_{10} core modes can be excited, respectively, at optimized periods and grating lengths with a tunable central wavelength, at the launch of the TM cladding mode. The periods of the needed SiON gratings are all over 2 μm, which is feasible with i-line UV lithography. Our results provide a low-cost edge coupler for LNOI photonic circuits with the ability of flexible spatial mode selectivity, which may promote LNOI devices in large-scale multiport photonic integrated circuits in the future.

Keywords: lithium-niobate-on-insulator chip; edge coupler; mode selectivity.

DOI: 10.3788/COL202523.013603

1. Introduction

Lithium-niobate-on-insulator (LNOI) devices have developed rapidly in the past decades, benefitting from fast-growing fabrication technologies[1–4]. Its excellent electro-optical and nonlinear optical features have promised bottleneck breakthroughs in electro-optical modulators[5–8], integrated lasers[9–11], nonlinear wavelength converters[12–14], quantum sources[15–18], etc., and may lead to revolutions in optical communication, microwave photonics, and quantum integration applications. Toward this, one of the remaining unsolved tasks is to design and fabricate efficient edge couplers for fiber-chip coupling and packaging for plug-and-play applications, with mode-selective excitation. Previously, several kinds of high-efficiency edge couplers have already been developed by means of adiabatic evolution[19–24]. However, they mainly focus on excitation of the first-order fundamental mode and lack flexibility for on-demand mode-selective excitations, including those of different polarization patterns, mode numbers, wavelengths, etc.

To obtain on-demand coupling of a certain mode, the exciting and required modes should be phase-matched and have non-zero spatial overlap at the cross-section plane. Different from traditional photonic integrated circuits (PICs), the mode field diameter (MFD) of the strong confined LNOI waveguide is only around 1 μm^2, which differs a lot from fibers. To achieve higher coupling efficiency, usually a gradual LNOI waveguide with an MFD gradient that changed from the normal waveguide size to near-zero and a low-refractive-index cladding mode with an MFD matching that of fibers is necessary for adiabatic evolution design[23]. Such sub-wavelength structures increase the fabrication complexity and constrict the overall feasibility of the edge coupler to be phase-matched with various waveguide modes, as limited by mode hybridization[25]. Thus, usually only the fundamental mode of the LNOI waveguide can be excited directly, and

additional on-chip mode converters[26–28] based on etched-LN structures have to be used for transversing the fundamental mode to the desired modes, which limits the flexibility of multi-mode applications and potential promotion of large-scale integrations.

Here, we design a new type of edge coupler with direct mode-selective excitation ability, using SiON cladding grating structures. A SiON cladding layer with periodic structures is introduced on a uniform LNOI waveguide for high-efficient butt-coupling to fibers and direct excitation of multiple core waveguide modes simultaneously. A cladding waveguide is fabricated on the edge of the cladding layer to provide a guided mode with an MFD that matches that of lens fibers for high-efficiency butt-coupling. Then periodic structures are introduced into the cladding layer to compensate for the momentum mismatch between the co-propagating guided mode and the desired LNOI waveguide mode so that the desired waveguide mode can be excited directly with high efficiency. Specifically, we provide a typical example of a Z-cut LNOI waveguide with a thickness of 600 nm, an etch depth of 350 nm, and a width of 1.4 μm. At the launch of the TM cladding mode, TM_{00}, TE_{00}, and TE_{10} core waveguide modes can be excited, respectively, at optimized period and grating length with a tunable central wavelength. The period of the SiON gratings is calculated to be all over 2 μm, which can be processed by mature i-line UV exposure. The results provide a compact and low-cost mode-selective edge coupler for the LNOI platform, which may be beneficial for large-scale multi-port PICs.

2. Results and Discussion

The scheme of the edge coupler is shown in Fig. 1. It consists of a SiON cladding layer with a grating structure above the LNOI ridge waveguide and the outermost SiO_2 protecting layer. Our design is based on a Z-cut LNOI wafer, with a 600-nm-thick $LiNbO_3$ thin film bonded on a 2-μm-thick thermally grown SiO_2 layer above a Si substrate. In order to reduce the propagation loss, we assume that 350 nm is etched to form the ridge waveguide, with a top width of 1.4 μm and a sidewall angle of 60°. The refractive index of SiON (~1.56) is larger than that of SiO_2 (~1.44), hence supporting the cladding mode in the SiON layer. The size of the SiON cross-section is designed to be 2.7 μm × 3 μm so that the cladding mode in SiON possesses a similar MFD (~2.8 μm) with lensed fiber (~2.0 μm), which allows efficient butt-coupling. In the SiON grating region, the reciprocal vector compensates for the wave vector mismatch between the cladding mode and the core mode so that the cladding mode can be efficiently coupled to the core mode during propagation.

To realize efficient coupling between the cladding mode in SiON and the core mode in $LiNbO_3$, the grating is used to compensate for their momentum mismatch. The grating period Λ is calculated as[29]

$$\Lambda = \frac{\lambda}{n_{\mathrm{eff,core}} - n_{\mathrm{eff,cladding}}}, \tag{1}$$

where $n_{\mathrm{eff,core}}$ and $n_{\mathrm{eff,cladding}}$ are effective indices of the core mode in the $LiNbO_3$ layer and the cladding mode in SiON, respectively. We choose the fundamental TM mode in the SiON cladding as the input mode in all the simulations below. In the waveguide we use here, we discuss three core modes TM_{00}, TE_{00}, and TE_{10}, and the grating periods for mode coupling between the cladding mode and these modes under different wavelengths are shown in Fig. 2(a). Aside from momentum conservation, the modal overlap also remarkably affects the coupling between modes. The field distributions of the three core modes and the TM cladding mode are shown in Fig. 2(b). It is noted that the TM cladding mode has horizontal symmetry in E_z and anti-symmetry in E_y. TM_{00} and TE_{10} core modes have the same symmetrical characteristics as TM cladding mode, and the mode overlap is non-zero between these core modes and the cladding mode. So the conversion from TM cladding mode to TM_{00} and TE_{10} core modes is supported directly in this structure. Meanwhile, TE_{00} has the opposite horizontal symmetry of the TM cladding mode, implying near-zero overlap. It means that coupling between the TE_{00} core mode and the TM cladding mode hardly occurs in this scheme. However, such mismatches

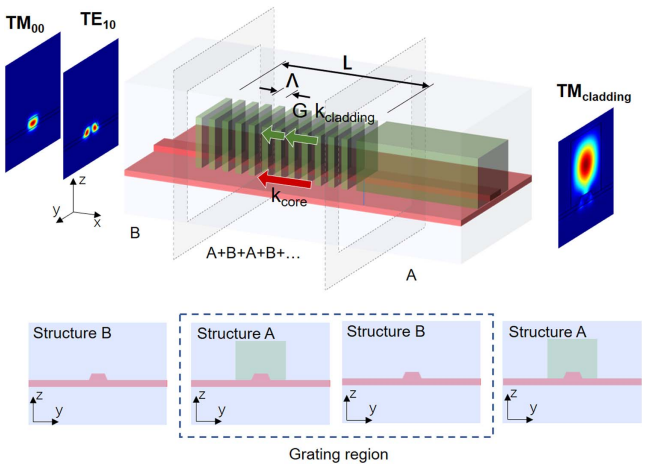

Fig. 1. Schematic of the LNOI edge coupler with cladding grating. Top panel: 3D schematic structure and principle of the grating edge coupler. Bottom panel: cross-sections at different positions.

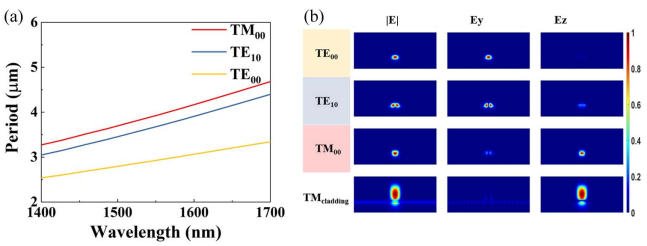

Fig. 2. Phase-matching condition and modal distributions. (a) Grating period Λ for momentum compensation at different wavelengths. (b) Modal distributions of the TM cladding mode and TM_{00}, TE_{10}, and TE_{00} core modes at 1550 nm.

can be dealt with using unsymmetric gratings, which we will discuss later.

The conversion from TM cladding mode to TM_{00} core mode simulated by the eigenmode expansion (EME) solver is shown in Fig. 3. Here we input the TM cladding mode at the right-side surface of the cladding layer as the light source, as shown in Fig. 1. For the central wavelength of 1550 nm, the grating period is optimized to be 4.041 μm. Because the phase-mismatch between the two modes is compensated exactly by the grating, the energy is coupled between the TM cladding mode and TM_{00} core mode periodically along propagation [Fig. 3(a)]. The maximum conversion occurs at the position $L = 18\Lambda$, with a conversion efficiency of 82%. Such coupling efficiency is comparable to other edge couplers[23,30–32]. Since it only requires a micrometers structure, it can hence be fabricated via low-cost i-line UV exposure technology. The conversion spectrum in Fig. 3(b) shows the 3 dB bandwidth of 42.0 nm. Note that the effective index of TE_{10} is close to that of TM_{00} mode, and a slight conversion to TE_{10} mode can be seen simultaneously in this case. However, at the grating period of 4.041 μm, TM_{00} possesses the most efficient conversion at 1550 nm, while TE_{10} conversion occurs at around 1592 nm. Since the region of TE_{10} conversion is far from that of TM_{00} coupling in the wavelength, it has a limited influence on the conversion efficiency of TM_{00}. As a result, the mode suppression ratio (MSR) of TM_{00} to TE_{10} is 20.2 dB at 1550 nm. We also simulate the conversion efficiency evolution of TM_{00} core mode at different wavelengths to further characterize its conversion bandwidth, as shown in Fig. 3(c). The results show a good performance in the first grating period. We also simulate the mode evaluation from TE cladding to TE_{00} to study the polarization sensitivity of this coupler. As shown in Fig. 3(b), the conversion efficiency is very low at wavelengths from 1400 to 1700 nm, showing that our coupler is polarization-sensitive.

Using the same structure, the conversion from TM cladding mode to TE_{10} core mode is simulated similarly, and the results are shown in Fig. 4. For efficient coupling at the 1550 nm, the grating period is optimized to be 3.875 μm. Figure 4(a) depicts the periodic energy conversion from TM cladding mode to TE_{10} core mode, and the maximum conversion occurs at the position $L = 75\Lambda$, with a conversion efficiency of 61%. It is noted that TM_{00} conversion also happens simultaneously in this case. The 3 dB bandwidth of TE_{10} conversion is 11.3 nm as shown in Fig. 4(b). At the period of 3.875 μm, TE_{10} possesses the most efficient conversion at 1550 nm, while TM_{00} conversion occurs at a wavelength near 1515 nm, which is in agreement with the phase-matching condition in Fig. 2(a). It is noted that TM_{00} has a much broader conversion bandwidth than TE_{10} because of the stronger modal overlap and, thus, easy coupling between TM_{00} core mode and TM cladding mode. Such a feature also leads to the mixture of TM_{00} in TE_{10}. As a result, the MSR between TE_{10} and TM_{00} is 8.91 dB at 1550 nm, as shown in Fig. 4(b). This MSR can be improved by increasing the propagation length, where the TE_{10} peak near $L = 225\Lambda$ has a higher MSR of 10.2 dB. This result demonstrates that, with a proper grating period, the long-period grating coupler can convert the cladding mode to a high-order core mode in even perpendicular polarization on demand, showing the mode-excitation flexibility of such a coupler.

Then we study the wavelength tunability of the edge coupler. The conversion efficiency of different wavelengths from the TM cladding mode to TM_{00} and TE_{10} core modes at three typical periods are simulated and shown in Fig. 5. When the period is changed from 3.823 to 4.248 μm, the central wavelength of TM_{00} conversion is tuned from 1500 to 1600 nm, demonstrating that our design can cover the whole S-C-L band. For TE_{10} mode, with the grating period changed from 3.662 to 4.084 μm, we can cover the wavelength from 1500 to 1600 nm as well [Fig. 5(b)]. The results demonstrate a flexible tunability of the resonant wavelengths.

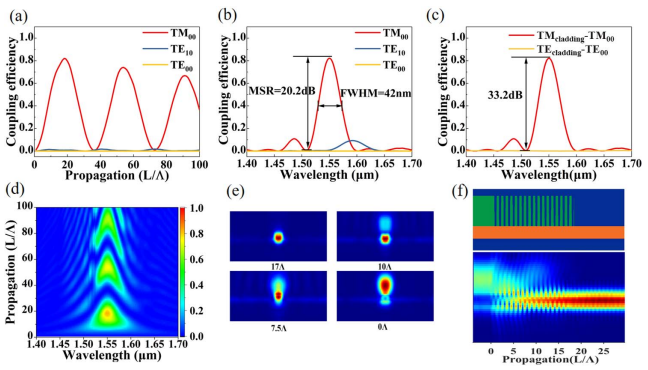

Fig. 3. Design for TM_{00} coupling at 1550 nm. (a) The conversion efficiency along with the propagation at the period of 4.041 μm and the wavelength of 1550 nm. (b) Conversion spectrum at the position of 18Λ. (c) Efficiency spectra of conversions from TE cladding to TE_{00} and TM cladding to TM_{00} at the position of 18Λ. (d) The conversion efficiency evolution of TM_{00} at different wavelengths. Electric field evolution of the TM cladding mode in (e) *x*–*z* and (f) *y*–*z* planes.

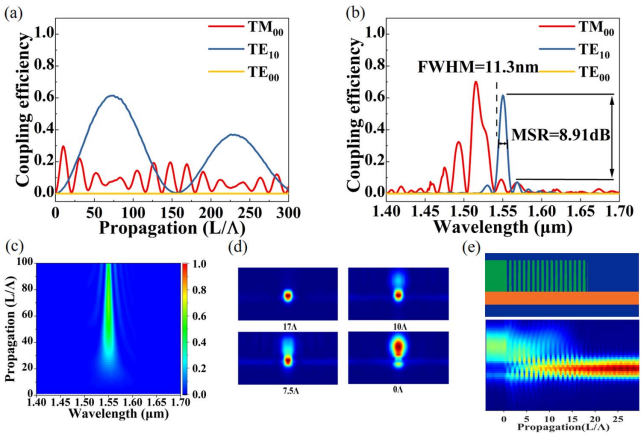

Fig. 4. Design for TE_{10} coupling at 1550 nm. (a) The conversion efficiency along with the propagation at the period of 3.875 μm and the wavelength of 1550 nm. (b) Conversion spectrum at the position of 75Λ. (c) The conversion efficiency evolution of TE_{10} at different wavelengths. Electric field evolution of the TM cladding mode in (d) *x*–*z* and (e) *y*–*z* planes.

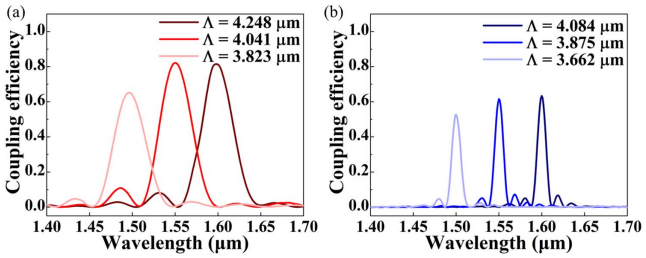

Fig. 5. Conversion spectra at three typical grating periods Λ. (a) TM_{00} mode. (b) TE_{10} mode.

Furthermore, as mentioned above, TE_{00} core mode has the opposite symmetrical characteristic of the TM cladding mode, which prohibits the coupling between the TE_{00} core mode and the TM cladding mode. To enhance the coupling between them, we broke the symmetry of the grating structure. Herein an asymmetric grating is proposed to realize TE_{00} conversion as shown in Fig. 6. In this scheme, the SiON is etched at either the left or right side in turns period by period, which leads to non-zero overlap between the TM cladding mode and the TE_{00} core mode, and allows conversion between the two modes.

For the central wavelength of 1550 nm, the grating period in the structure is optimized to be 3.047 μm, and the energy conversion of TE_{00} mode along propagation is shown in Fig. 7(a). The maximum conversion occurs at the position $L = 635\Lambda$, with a conversion efficiency of 85%. The 3 dB bandwidth of the conversion spectrum is 1.55 nm, as shown in Fig. 7(b). Because the effective index of TE_{00} is far from those of TE_{10} or TM_{00} modes, energy is hardly coupled to the TE_{10} or TM_{00} mode. The MSR of TE_{00} to TE_{10} is 35.2 dB at 1550 nm, which implies the high purity of TE_{00} mode conversion.

For this asymmetric cladding grating coupler, we also study its wavelength tunability. As shown in Fig. 8, when the period is changed from 2.922 to 3.172 μm, the central wavelength of

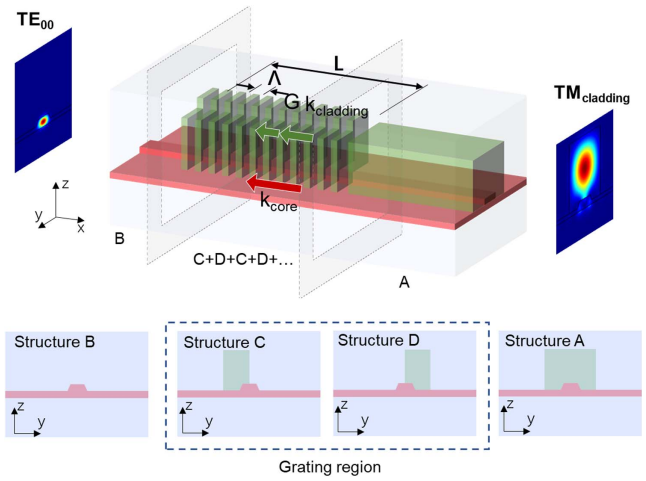

Fig. 6. Schematic of the LNOI edge coupler with asymmetric cladding grating. Top panel: 3D schematic structure. Bottom panel: cross-sections at different positions.

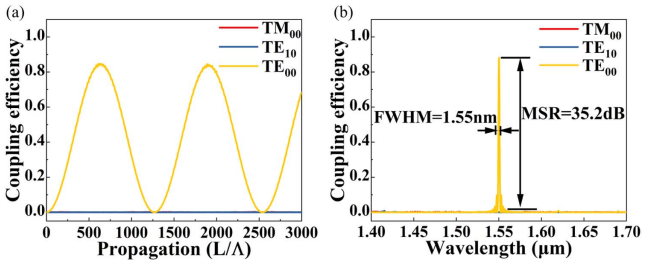

Fig. 7. Design for TE_{00} coupling at 1550 nm. (a) Conversion efficiency along with the propagation at the period of 3.047 μm and the wavelength of 1550 nm. (b) Conversion spectrum at the position of 635Λ.

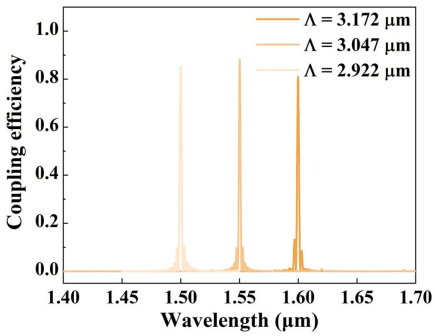

Fig. 8. Conversion spectra at different grating periods Λ for TE_{00} mode.

TE_{00} conversion is tuned from 1500 to 1600 nm, which also covers the whole S-C-L band.

3. Conclusion

In conclusion, we have proposed a new type of edge coupler for LNOI devices using SiON cladding grating structures to realize efficient fiber-chip coupling and selectively excite distinct spatial modes simultaneously. For a typical example of C-band coupling here, the needed grating period is calculated to be over 2 μm, which is feasible with i-line UV lithography. At the launch of the TM cladding mode, TM_{00} waveguide mode can be excited with maximum coupling efficiency exceeding 85%, and the maximum 3 dB bandwidth reaches 42 nm. With further optimization via a chirp grating structure or dispersion-engineered waveguide, the coupler bandwidth can be further increased. The excitation of high-order TE_{10} waveguide mode can also be realized directly using the same structure with optimized parameters. By breaking the symmetry of the coupler's grating, the conversion of TM cladding mode to TE_{00} waveguide mode is achieved with high efficiency, enabling direct polarization-rotating during the fiber-chip coupling. Compared to on-chip mode converters, our coupler can achieve efficient fiber-chip coupling and mode excitation to the specific core mode simultaneously using a single device; hence, it is a more compact choice for mode-selected excitation from fiber to chip. Furthermore, by controlling the grating period, the central wavelength of the

excited modes can be easily tuned to cover the whole S-C-L band. Our results provide a low-cost coupler for LNOI PICs with spatial mode selectivity, which will be helpful for plug-and-play applications in optical communication, microwave photonics, and quantum integration areas.

Acknowledgements

This work was supported by the National Key R&D Program of China (Nos. 2022YFA1205100 and 2019YFA0705000), the National Natural Science Foundation of China (Nos. 62293523, 12304421, and 62305156), the Jiangsu Natural Science Foundation (No. BK20232033), the Leading-edge Technology Program of Jiangsu Natural Science Foundation (No. BK20192001), the Zhangjiang Laboratory (No. ZJSP21A001), and the Jiangsu Funding Program for Excellent Postdoctoral Talent.

References

1. A. Boes, L. Chang, C. Langrock, *et al.*, "Lithium niobate photonics: unlocking the electromagnetic spectrum," Science **379**, eabj4396 (2023).
2. B. Leah, "Now entering, lithium niobate valley," https://seas.harvard.edu/news/2017/12/now-entering-lithium-niobate-valley (December 21, 2017).
3. G. Chen, N. Li, J. D. Ng, *et al.*, "Advances in lithium niobate photonics: development status and perspectives," Adv. Photon. **4**, 034003 (2022).
4. Z. Xie, F. Bo, J. Lin, *et al.*, "Recent development in integrated lithium niobate photonics," Adv. Phys. X **9**, 2322739 (2024).
5. C. Wang, M. Zhang, X. Chen, *et al.*, "Integrated lithium niobate electro-optic modulators operating at CMOS-compatible voltages," Nature **562**, 101 (2018).
6. M. He, M. Xu, Y. Ren, *et al.*, "High-performance hybrid silicon and lithium niobate Mach–Zehnder modulators for 100 Gbit s−1 and beyond," Nat. Photonics **13**, 359 (2019).
7. P. Kharel, C. Reimer, K. Luke, *et al.*, "Breaking voltage-bandwidth limits in integrated lithium niobate modulators using micro-structured electrodes: erratum," Optica **8**, 1218 (2021).
8. M. Xu, Y. Zhu, F. Pittalà, *et al.*, "Dual-polarization thin-film lithium niobate in-phase quadrature modulators for terabit-per-second transmission," Optica **9**, 61 (2022).
9. V. Snigirev, A. Riedhauser, G. Lihachev, *et al.*, "Ultrafast tunable lasers using lithium niobate integrated photonics," Nature **615**, 411 (2023).
10. M. Yu, D. Barton Iii, R. Cheng, *et al.*, "Integrated femtosecond pulse generator on thin-film lithium niobate," Nature **612**, 252–258 (2022).
11. M. Li, L. Chang, L. Wu, *et al.*, "Integrated Pockels laser," Nat. Commun. **13**, 5344 (2022).
12. P.-K. Chen, I. Briggs, C. Cui, *et al.*, "Adapted poling to break the nonlinear efficiency limit in nanophotonic lithium niobate waveguides," Nat. Nanotechnol. **19**, 44–50 (2024).
13. M. G. Vazimali and S. Fathpour, "Applications of thin-film lithium niobate in nonlinear integrated photonics," Adv. Photon. **4**, 034001 (2022).
14. J. Zhao, M. Rüsing, U. A. Javid, *et al.*, "Shallow-etched thin-film lithium niobate waveguides for highly-efficient second-harmonic generation," Opt. Express **28**, 19669 (2020).
15. S. Saravi, T. Pertsch, and F. Setzpfandt, "Lithium niobate on insulator: an emerging platform for integrated quantum photonics," Adv. Opt. Mater. **9**, 2100789 (2021).
16. J. Lu, M. Li, C.-L. Zou, *et al.*, "Toward 1% single-photon anharmonicity with periodically poled lithium niobate microring resonators," Optica **7**, 1654 (2020).
17. H.-Y. Liu, M. Shang, X. Liu, *et al.*, "Deterministic N-photon state generation using lithium niobate on insulator device," Adv. Photon. Nexus **2**, 016003 (2022).
18. G.-T. Xue, Y.-F. Niu, X. Liu, *et al.*, "Ultrabright multiplexed energy-time-entangled photon generation from lithium niobate on insulator chip," Phys. Rev. Appl. **15**, 064059 (2021).
19. L. He, M. Zhang, A. Shams-Ansari, *et al.*, "Low-loss fiber-to-chip interface for lithium niobate photonic integrated circuits," Opt. Lett. **44**, 2314 (2019).
20. C. Hu, A. Pan, T. Li, *et al.*, "High-efficient coupler for thin-film lithium niobate waveguide devices," Opt. Express **29**, 5397 (2021).
21. P. Ying, H. Tan, J. Zhang, *et al.*, "Low-loss edge-coupling thin-film lithium niobate modulator with an efficient phase shifter," Opt. Lett. **46**, 1478 (2021).
22. N. Yao, J. Zhou, R. Gao, *et al.*, "Efficient light coupling between an ultra-low loss lithium niobate waveguide and an adiabatically tapered single mode optical fiber," Opt. Express **28**, 12416 (2020).
23. X. Liu, S. Gao, C. Zhang, *et al.*, "Ultra-broadband and low-loss edge coupler for highly efficient second harmonic generation in thin-film lithium niobate," Adv. Photon. Nexus **1**, 016001 (2022).
24. D. Jia, Q. Luo, C. Yang, *et al.*, "High-efficiency edge couplers enabled by vertically tapering on lithium-niobate photonic chips," Appl. Phys. Lett. **123**, 263502 (2023).
25. A. Kaushalram, G. Hegde, and S. Talabattula, "Mode hybridization analysis in thin film lithium niobate strip multimode waveguides," Sci. Rep. **10**, 16692 (2020).
26. G. Yang, A. V. Sergienko, and A. Ndao, "Tunable polarization mode conversion using thin-film lithium niobate ridge waveguide," Opt. Express **29**, 18565 (2021).
27. Y. Shen, Z. Ruan, K. Chen, *et al.*, "Broadband polarization splitter-rotator on a thin-film lithium niobate with conversion-enhanced adiabatic tapers," Opt. Express **31**, 1354 (2023).
28. X. Liang, L. Fu, Q. Yu, *et al.*, "Efficient and broadband trident spot-size convertor for thin-film lithium niobate integrated device," IEEE Photon. Technol. Lett. **35**, 35–38 (2023).
29. V. Rastogi and K. S. Chiang, "Long-period gratings in planar optical waveguides," Appl. Opt. **41**, 6351 (2002).
30. K. Shiraishi, H. Yoda, A. Ohshima, *et al.*, "A silicon-based spot-size converter between single-mode fibers and Si-wire waveguides using cascaded tapers," Appl. Phys. Lett. **91**, 141120 (2007).
31. J. Zhang, X. Shi, Z. Zhang, *et al.*, "Polarization-insensitive ultra-short waveguide taper," Opt. Lett. **46**, 5027 (2021).
32. Y. Li, T. Lan, J. Li, *et al.*, "High-efficiency edge-coupling based on lithium niobate on an insulator wire waveguide," Appl. Opt. **59**, 6694 (2020).